

Three-level multi-scale modeling of electrical contacts

sensitivity study and experimental validation

*Vladislav A. Yastrebov, Georges Cailletaud,
Henry Proudhon*

MINES ParisTech, PSL Research University, Centre des
Matériaux, CNRS UMR 7633
Evry, France

vladislav.yastrebov@mines-paristech.fr
georges.cailletaud@mines-paristech.fr
henry.proudhon@mines-paristech.fr

*Frederick S. Mballa Mballa, Sophie Noël,
Philippe Testé, Frédéric Houzé*

Laboratoire Génie électrique et électronique de Paris,
UMR CNRS-CentraleSupélec 8507, UPMC and Paris-Sud
Universities, Gif sur Yvette, France

sophie.noel@geeps.centralesupelec.fr
philippe.teste@geeps.centralesupelec.fr
frederic.houze@geeps.centralesupelec.fr

Abstract—An experimental and numerical study of electrical contact for low currents in sphere-plane set-up is presented. A three-level multi-scale model is proposed. We use the finite element analysis for macroscopic mechanical and electric simulations. It takes into account the setup geometry, elasto-plastic mechanical behavior of contacting components in the finite-strain-plasticity framework and electrostatic properties. A sensitivity analysis with respect to the brass plastic behavior and to the thickness of coating layers is also performed. The finite element results are used for an asperity-based model, which includes elasto-plastic deformation of asperities and their mutual elastic interactions. This model enables us to simulate the real morphology of contact spots at the roughness scale using the experimentally measured surface topography. Finally, the Greenwood multi-spot model is used to estimate the electrical contact resistance. This three-level model yields results which are in good agreement with experimental measurements carried out in this study.

Keywords: *electrical contact, elasto-plastic material, experimental measurements, multi-scale simulations.*

I. INTRODUCTION

Electrical contacts can be critical components in electronic systems. Their electrical resistance and life duration depend on many factors such as life cycles, interaction with the environment (oxidation and corrosion), surface morphology, surface chemistry and bulk material electrical properties and mechanical behavior. In this paper we study both experimentally and numerically the influence of the materials properties and the geometry of the coating layers on the electrical contact resistance between a copper-beryllium sphere indenting a brass flat substrate coated with nickel and gold.

Electrical contacts performances and reliability critically depend on the characteristics and evolution of the so-called real area of contact, composed of numerous zones whose size and distribution are determined by the macroscopic shape of bodies, the roughness of their surfaces, their mechanical and electric properties as well as by mechanical loads and involved electric currents. Contact resistance mainly results from the constriction of current lines at these contacting spots. A project has been set-up joining the efforts of two laboratories in the fields of experimental and numerical studies to clarify the

interplay of multiscale and multiphysics mechanisms in this complex interfacial region.

Phenomenon of electrical contact combines mechanical and electric effects, as the electric current can pass mainly through contact spots which result from mechanical deformation of contacting solids. Thus, if the coupling between the mechanical and electric effects may be assumed unidirectional (which is often the case for low currents and moderate loads) then this coupled problem can be split in two sub-problems: first, the mechanical contact problem, second, the electrostatic problem for the geometry obtained from the solution of the first. With this consideration in hand, one can combine independent models for mechanical and electrical contacts. For the latter, the simplest model consists in approximation of the real conducting zone by a single circular conducting spot at the interface between semi-infinite planes [1]; for the case of two finite cylinders contacting at a circular spot, first terms in the Taylor's expansion of the solution were obtained in [2]. A generalization of these simple models is the multi-spot Greenwood model [3], which approximates the contact interface by a cluster of conducting circular spots at the interface between two conducting half-spaces. Some further generalizations of this model are also available in the literature, including models which take into account aging of contact spots prone to the growth of oxide films [4], models considering the current density distribution inside contact spots [5], models adapted for saturated contacts, when the electrical contact area approaches the apparent contact area while the number of contact spots remains small [6], models including interface film resistance [7] and smoothed version of Greenwood model, which represents the discrete sums by integrals with specific kernels [8].

Equivalently many models exist to solve the mechanical contact between rough surfaces, whose solution determines the morphology of the mechanical contact area, which may be considered as the upper boundary for the electrical contact area [9]. Among these models there are analytical asperity-based models [10-13], which approximate the effective roughness of two contacting surfaces by a series of spherical or ellipsoidal non-interacting asperities, with specific distribution of their geometrical properties, which in turn follow the random process roughness model developed in [14,15]. A multiscale

generalization of asperity based models is suggested in [16], which assumes however a kind of scale separation in the surface roughness. A different approach is developed in [17], which considers a full contact for varying spectral content as a starting point, and next extends the result for the case of partial contacts [18]. These models, associated approximations, limitations and possible extensions are summarized in [19,20]. Apart from these analytical and semi-analytical models, various numerical methods may be used to solve the mechanical boundary value problem with contact constraints and explicitly integrated surface roughness for elastic [21-23], visco-elastic [24] and elasto-plastic material models [25,26]. Different approaches and results of these full-scale analyses are summarized in [27].

In weakly coupled electro-mechanical contact problems, the multiscale and multiphysics model is essentially a combination of one of aforementioned mechanical and electrical models. It is worth mentioning that the mechanical part is sometimes simply neglected and the spot distribution is either simulated by a random model or is obtained as a cross-section of a rough surface (geometrical overlap model), see e.g. [8,28,29]. We refer to following references [30-34], as to the state of the art works, in which more complete and accurate models are used for mechanical and electrical contacts. Moreover, in [34] a link of aforementioned models with a rather different, incremental stiffness approach of Barber is discussed [35]. In conclusion of the bibliographical review, it should be remarked that the electrical contact problem is essentially similar to the one of thermal conductance through the same configuration of contact spots, under condition that the thermal expansion of solids and convective heat exchange are neglected. Hence, a rich bibliography on thermal contact conductance [36,37] is partly relevant to our topic.

Our work combines within a unified framework several numerical models for mechanical and electrical contacts. A mechanical finite element model, which uses accurate constitutive equations to capture elasto-plastic material behavior, allows us to predict the structural response for complex loading including cyclic loads in contact. An improved elasto-plastic asperity model with elastic interactions between asperities is then used to capture the roughness effect using the real topography of our samples measured with atomic force microscopy. This model provides us with statistically meaningful results and allows us to estimate the data dispersion. Finally, the original Greenwood model is used to analyze the electrical resistance of contact clusters. This model is validated on a series of fine experiments conducted in the project.

In Section II, the general methodology is described. Section III presents the experimental setup and corresponding measurements. The numerical approach (finite element analysis) as well as the mechanical constitutive models which are used in the simulations are discussed in Section IV. The roughness of the contacting surfaces is analyzed in Section V; the multi-scale electro-mechanical model and the associated results are presented in Section VI, followed by a discussion.

II. METHODOLOGY

The general objective of the study is to predict the experimentally observed variation of the electrical contact resistance for “real” sphere-plane contacts under cyclic

loadings using multiscale electro-mechanical simulations. To reach this objective, we integrate in the numerical model (1) realistic constitutive material models (elasto-plastic with isotropic and kinematic hardening), (2) an accurate representation of the roughness morphology of the contacting bodies as measured by atomic force microscopy (AFM) and interferometric profilometry. The multiscale nature of the electric and mechanical contact manifests itself in a separation of scales between the macroscopic geometry of the contacting solids and the microscopic roughness on a smaller scale (Fig. 1). In our study we use this scale separation in the following way. First, we conduct the mechanical simulation of the indentation for various materials and coating thicknesses assuming perfectly smooth surfaces (with no roughness). At every load step, a complementary electrostatic simulation is conducted to evaluate the electrical contact resistance. Both simulations are carried out using a finite element software with implicit integration [38,39]. The effect of the roughness and of the microscopic deformation of asperities is then taken into account in a semi-analytical model of interacting asperities, which uses the real roughness topography. This model provides us with the exact morphology of the contact spots, which is then used to estimate the contact resistance via the Greenwood model (Eq. (4) in [3]). The sensitivity of the mechanical model with respect to material properties (initial yield stress) and to the thickness of coating layers is then analyzed. The numerical results are compared with the experimental data.

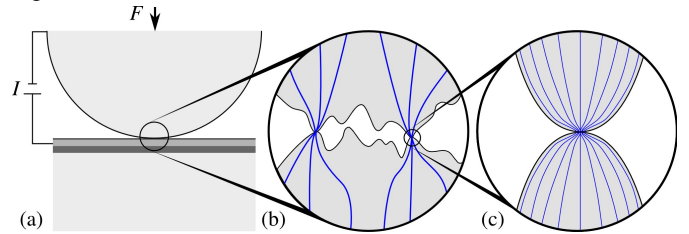


Fig. 1. Separation of scales in the electric and mechanical contact between rough solids: (a) the macroscopic scale is characterized by nominally flat (smooth) surfaces, (b) at certain magnification the discrete nature of the contact is revealed. The real contact area is considerably smaller than the nominal contact area predicted at macroscopic scale with the Hertz contact theory; the real contact area can be approximated by a set of a-spots (c).

III. SAMPLES AND EXPERIMENTAL SET-UP

Cyclic indentation tests were performed on nominally flat substrates by a copper beryllium ball of radius 1.75 mm. The flats were one millimeter thick brass alloy CuZn30 [CW505L, 30 wt% Zn] planes coated with electrodeposited nickel and gold layers both $1\mu\text{m}$ thick. Bare CuBe balls were used. Particular attention was devoted to their surface. Several types of experiments involving different surface finishes of the balls were performed. The balls were either rinsed, thoroughly cleaned or mechanically polished before the measurements. The experiments were conducted on a special test bench depicted in Fig. 2. The ball is mounted in a holder and pressed against the plate with a stepping actuator ($1/10\mu\text{m}$ by step), which is controlled by a displacement capacitive sensor (a preliminary calibration procedure permits to convert the

vertical displacement into the value of the normal force via the stiffness of the guiding elastic rings). A water-cooling circuit insures the thermal stability of the set-up, specifically the sensor's measurements. The elements of the contact are connected to the electrical setup following the four-terminal method. The electrical circuit includes a DC voltage/current source, an electrometer and a digital voltmeter, all controlled over the IEEE-488 bus. Once the required force is reached, a DC current $I = 10\text{mA}$ is imposed to the contact; opposite polarities are used to eliminate thermoelectric voltages (current-reversal method) [40]. Measurements of the potential difference (U) enable us to calculate the total electric resistance

$$R = R_c + R_s = U/I \quad (1)$$

where R_c is the contact resistance and R_s is an additional resistance due to the bulk parts of ball-holder and brass plane between contact area and potential measurement terminals. In the considered system R_s is estimated to be about $0.09\text{ m}\Omega$. Under assumption of elastic Hertzian contact and Holm's electrical contact, the first term can be estimated as follows:

$$R_c = \frac{\rho^*}{2a} = \frac{\rho^*}{2} \left(\frac{4E^*}{3RF} \right)^{1/3} \quad (2)$$

where R is the ball radius, a is the contact radius, ρ^* the effective resistivity, E^* the effective modulus, and ρ^* is usually taken as a mean resistivity of CuBe and CuZn. The effective elastic modulus is considered for the pair CuBe and CuZn

$$\frac{1}{E^*} = \frac{1 - \nu_{\text{CuBe}}^2}{E_{\text{CuBe}}} + \frac{1 - \nu_{\text{CuZn}}^2}{E_{\text{CuZn}}} \quad (3)$$

where ν is the Poisson's ratio and E is the Young's modulus.

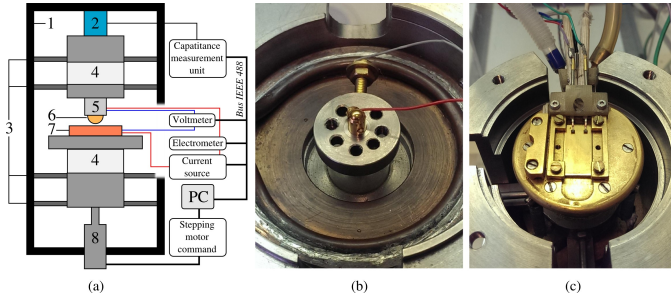


Fig. 2. (a) General layout of the contact resistance measurement setup: 1 – rigid frame, 2 – capacitive force sensor, 3 – elastic washers, 4 – insulating blocks, 5 – ball holder, 6 – CuBe ball, 7 – plane CuZn substrate coated with Ni and Au, 8 – displacement stepping motor. (b) Mounted CuBe ball, two wires (grey: current feeding, red: voltage measurement) and the water cooling system (tube); (c) sample holder for the plate (7) with connections.

Series of three loading-unloading cycles were performed in various conditions (ball finish and indentation zone). Experimental data for a representative test as well as the the range of experimental data obtained for different runs (shaded area) are depicted in Fig. 3 which shows the evolution of the measured resistance with respect to the applied load as well as the analytical estimation from Eq. (1,2). The first loading is observed to be distinct from the subsequent loading-unloading curves because of the plasticity onset in the CuZn substrate.

After the first hardening the system follows a stabilized cycle: the loading and unloading curves follow the same trajectories. The hysteresis is attributed to the kinematic hardening in CuZn. The variability in the experimental results can be explained by differences in the surface states of the balls (including roughness and contamination) and on the local roughness of the plane at the location of the indentation.

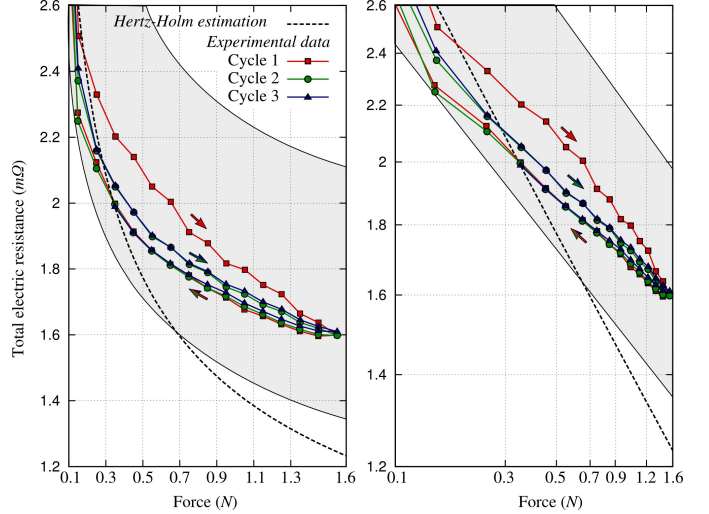


Fig. 3. Experimental data and analytical estimation: left – normal scale, right – logarithmic scale. Shaded area encloses all the experimental data points for the first three loading-unloading cycles for different ball finishes and at different locations on the plate. The data points show three cycles of a representative experiment; the dashed line shows a reference analytical estimation for elastic Hertzian contact Eq. (1,2) for $R_s=0.09\text{ m}\Omega$. Arrows with the color code indicate the load direction.

IV. NUMERICAL SIMULATIONS AND MATERIAL MODELS

The macroscopic calculation is made on an axisymmetric model, as shown in Fig. 4. A convergence study has been performed in order to choose the optimum element size in the contact zone. Linear elements are used in the finite element mesh to ensure an optimal contact treatment. The nickel and gold layers are discretized by two element layers in thickness. Elements in the vicinity of the contact have a size of 500 nm . The number of elements in contact reaches more than 80 at the peak load. A prescribed displacement is imposed on the equatorial plane of the half sphere (A in Fig.4), which remains flat due to a multi-point constraint condition, while the bottom of the mesh representing the substrate (B in Fig.4) is fixed in vertical direction. The mechanical simulation allows us to obtain the evolution of the radius of the contact surface with respect to the applied force. At each load step, the two initially separate meshes are fused in the contact zone for the computation of the electrical problem. Doing so, there is no discontinuity in electric potential at the boundary between the sphere and the plane. The electrical model at macroscopic scale thus assumes a perfect contact between the two bodies (no resistive interfacial film).

Non linear constitutive equations were used for the three materials of the substrate (CuZn, Au and Ni), while an elastic

behavior is considered for the ball CuBe material model. In each case, the material data are taken from literature (respectively [41,42] and [43] for brass, gold and nickel). The material models incorporate either only non-linear kinematic hardening (Au, Ni) or a combination of isotropic and several kinematic hardening (CuZn), in order to correctly represent cyclic responses of the materials. The expressions are summarized below, Eq.(4-9). The yield function, f , in Eq.(4) uses the von Mises invariant, denoted by J , of the effective stress (the stress minus the kinematic variable), as specified in Eq.(5). The size of the elastic domain is defined by the sum of the initial yield stress, σ_y , and the isotropic hardening variable, R . Two material parameters, namely the possible amount of hardening Q and the parameter characterizing the saturation rate, b , are present in Eq.(6) to define isotropic hardening. The expression of kinematic hardening has a driving term proportional to the plastic strain rate, and a fading memory term proportional to its actual value. The product $D\Phi(p)$ characterizes the non linearity of the stress evolution inside a cycle. Its initial value is D and the final $D\phi_\infty$, that allows representing a sharper hysteresis loop after a few cycles. The variable p brought into play in both Eq.(6) and Eq.(7) is the cumulated plastic deformation, defined by its rate, as shown in Eq.(9).

$$f(\underline{\sigma}, \underline{X}, R) = J(\underline{\sigma} - \underline{X}) - R - \sigma_y \quad (4)$$

$$J(\underline{\sigma} - \underline{X}) = \sqrt{3/2(\underline{s} - \underline{X}) : (\underline{s} - \underline{X})} \quad (5)$$

$$R = Q(1 - \exp(-bp)) \quad (6)$$

$$\dot{\underline{X}} = (2C/3)\dot{\underline{\epsilon}}^p - D\Phi(p)\underline{X}\dot{p} \quad (7)$$

$$\Phi(p) = \phi_\infty + (1 - \phi_\infty)\exp(-\omega p) \quad (8)$$

$$\dot{p} = \sqrt{(2/3)\dot{\underline{\epsilon}}^p : \dot{\underline{\epsilon}}^p} \quad (9)$$

where \underline{s} is the deviatoric part of the stress tensor $\underline{\sigma}$, the dot represents the time derivative and the colon represents tensor contraction.

A simple sensitivity analysis was carried out with respect to the yield stress of the brass: $53 \text{ MPa} < \sigma_y < 550 \text{ MPa}$ and to the thickness of both coating layers in the range $0.5 < h < 3.0 \text{ }\mu\text{m}$ (for fixed $\sigma_y=70 \text{ MPa}$). The results are shown in (Fig. 5). For the experimental range of loads used in the study, the yield stress determines:

- if the contact is purely elastic ($\sigma_y \approx 550 \text{ MPa}$),
- if the first load is elasto-plastic and the subsequent load cycles are elastic ($\sigma_y \approx 140 \text{ MPa}$),
- if a purely elasto-plastic case with no stabilized cycle is obtained ($\sigma_y \approx 53 \text{ MPa}$).

The parameters, which were identified from above-mentioned experiments [41-43] and used in the finite element and multiscale analyses, are summarized in Table I.

Note that our model cannot describe at the same time the experimental cycle with superposed second and third loadings as well as the first, second, and third unloading (Fig. 3). Since, such a hysteresis, as we believe, is associated with the brass

response, this result indicates that a finer characterization of the material behavior, specifically for conditions of cyclic loadings with a very large hydrostatic pressure is needed. The imprecision in experimental measurement of the thickness of both the Ni and Au coatings affects only marginally the results: the curves obtained for different thicknesses (not shown here) are very close to the reference one (both layers are $1 \text{ }\mu\text{m}$ thick).

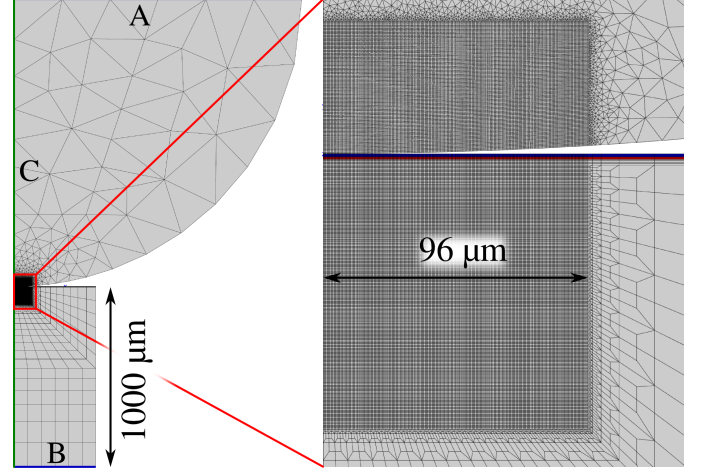


Fig. 4. Finite element mesh used for mechanical and electric simulations: general view and a zoom on the contact region with hardly visible nickel and gold layers of $1 \text{ }\mu\text{m}$ thickness each.

TABLE I. TABLE OF MATERIAL PARAMETERS

Parameter	Material / Value(s)			
	<i>Au</i>	<i>Ni</i>	<i>CuBe</i>	<i>CuZn30</i>
E (GPa)	70	160	130	110
ν	0.42	0.31	0.3	0.375
σ_y (MPa)	141	677	-	53, 70, 140, 550
b	-	-	-	1.18
Q (MPa)	-	-	-	20
C_1 (GPa)	122	333	-	35
D_1 (MPa)	332	251	-	1000
ϕ_1	1	1	-	0.02
ω_1	-	-	-	0.09
C_2 (GPa)	-	-	-	45
D_2 (MPa)	-	-	-	9550
ϕ_2	-	-	-	0.8
ω_2	-	-	-	9.8
C_3 (GPa)	-	-	-	70
D_3 (MPa)	-	-	-	10500
ϕ_3	-	-	-	0.7
ω_3	-	-	-	5.5
ρ (Ohms· μm)	2.33e-2	6.99e-2	8.25e-2	6.2e-2

V. SURFACE ROUGHNESS

The coated brass flats roughness was characterized by AFM and profilometry. It cannot be described as self-affine fractal with a single Hurst exponent (or fractal dimension). Fig. 6 shows that it is a combination of the roughness naturally present in rolled brass alloys and the roughness of electrodeposited nickel and gold layers. The coated substrate topography (AFM data, 5 scans 2048x2048 points) can be characterized by its power spectral density (PSD) in two

orthogonal directions and by the height distribution; both are depicted in Figs. 7-8, respectively.

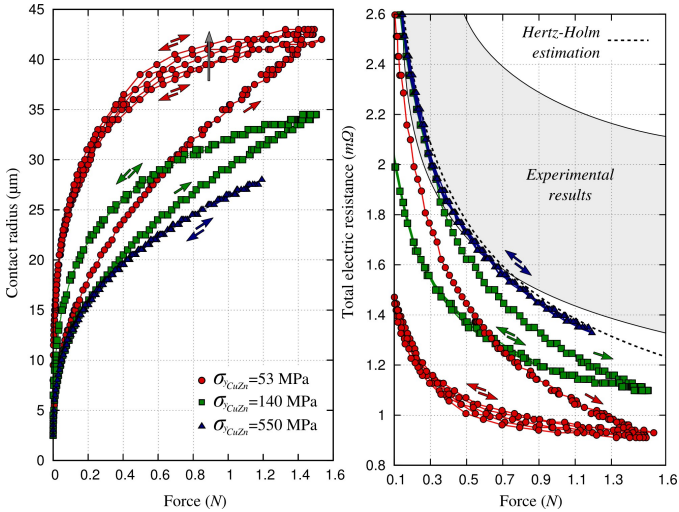


Fig. 5. Results of finite element analysis: contact radius (left) and electric resistance (right) evolution in cycling loading. The shaded area spans all experimental results and the dashed line is the reference analytical estimation for elastic Hertzian contact Eq. (1,2) computed for $R_s=0.09$ mΩ.

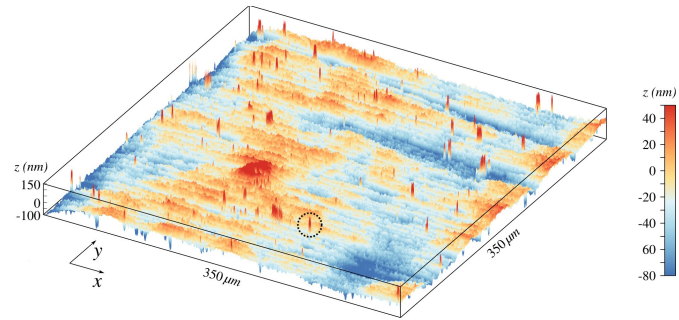


Fig. 6. Example of roughness measurements (AFM) on the coated brass substrate.

The roughness is observed to be anisotropic (mainly because of the rolling) with a particular scaling in terms of the PSD; the height distribution is not Gaussian, with a rather pronounced tail, which arises due to numerous high asperities (see Fig. 8). Rigorously, such a surface cannot be analyzed by standard methods of the random process model [14,15,44]. It should be noted that the surface anisotropy does not imply a strong anisotropy of asperities, equivalently the isotropy of the surface does not imply the isotropy of asperities. As was shown in [45], according to the random process model, the mean ratio of asperity principal curvatures is approximately three and the probability to find a circular asperity is zero.

The surface roughness was analyzed numerically. First the data were filtered in Fourier space by a low pass cut-off filter at $|k|=512$. Next the data were processed to identify all asperities and their relevant properties: in-plane coordinate x,y , peak height z and principal curvatures κ_1,κ_2 . These data were then used in the following section to obtain the realistic contact morphology (real contact area) for different loads and

various indentation zones. Note that the roughness of the ball is not included here.

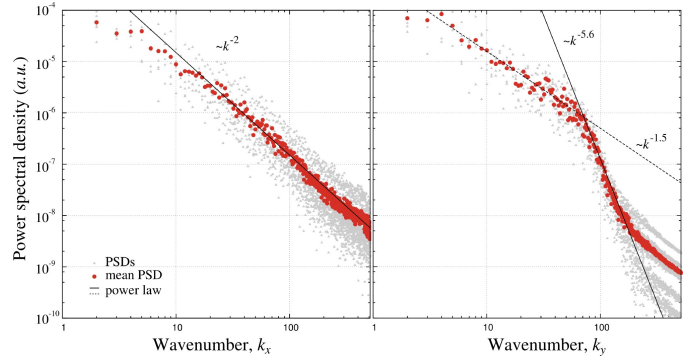


Fig. 7. Power spectral density of the surface roughness in the direction X (left) and Y (right): gray triangles represent all the measured surfaces, red circles correspond to the average data.

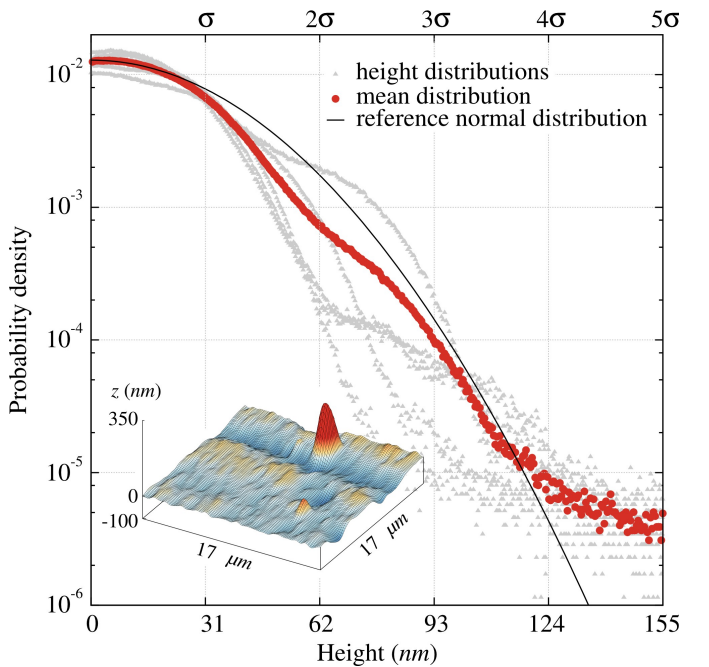


Fig. 8. Distribution of surface heights: gray triangles represent all the measured surfaces, red circles correspond to the average data. In the inset an example of a high asperity; whose population changes significantly the distribution tail.

VI. THREE-LEVEL MULTISCALE MODEL

A realistic estimation of the electrical contact resistance needs to take in consideration the roughness of the contacting surfaces. The approach in this work is based on the consecutive use of three computational tools:

- (1) a finite element analysis to solve the indentation problem for smooth coated substrate within finite strain plasticity framework;
- (2) a semi analytical iterative tool based on elasto-plastic deformation of elastically interacting asperities;

(3) Greenwood's model [3] to estimate the electrical contact resistance through a localized cluster of a -spots:

$$R_G = \frac{\rho^*}{2\pi \sum a_i} \left(\pi + 2 \frac{\sum_{i \neq j} \sum a_i a_j / s_{ij}}{\sum a_i} \right) \quad (10)$$

where a_i is the radius of the i -th contact spot and s_{ij} is the distance between centers of spots i and j .

In model (1) (described in detail in Section IV) for each value of the load F we obtain the contact radius a_0 and the pressure distribution in the contact zone $p(r)$, $r < a_0$. For small loads the contact pressure follows Hertzian distribution, for moderate loads accompanied with considerable plastic deformation, the contact pressure is almost uniform over the contact zone and can be estimated [46] as $p=3\sigma_y$, where σ_y is the yield stress of the substrate (we assume that CuBe ball remains in the elastic regime), for higher loads the plastic flow and large deformations change the contact pressure profile in a way that the contact pressure is higher near the edge of the contact zone. Model (1) is needed to take into account the plasticity at macroscopic scale, which is not possible in the asperity-based framework (2). To make a link between these two models, we make the following assumptions:

- (i) the apparent contact zone at the asperity scale lies within the contact radius a_0 obtained in model (1);
- (ii) the asperities (position, peak height, principal curvatures) are identified from real AFM topographies of the coated plane and they are assumed to be spherical with the geometrically mean curvature $\kappa = \sqrt{(\kappa_1 \kappa_2)}$;
- (iii) the asperities are indented by a flat circular punch of radius a_0 ;
- (iv) the deformation of the asperities is governed by the Hertz theory with effective elastic modulus computed for the combination of CuBe and Au;
- (v) to represent the irreversible plastic deformation of the asperities the maximal value of the mean contact pressure is fixed at $3\sigma_y$, where σ_y is the yield stress of Au;
- (vi) the elastic interaction between asperities is governed by the elastic constants of the substrate CuZn.

Under these assumptions and limitations, model (2) can be properly used only for the first loading as the change of the shape of asperities, their curvature and residual bulk deformation are non-trivial to take into account even being guided by model (1). Thus, our objective is to capture the variability of the resistance for the first loadings via statistically meaningful series of simulations, which will represent an upper limit for the resistance in the stabilized loading-unloading cycle. We then use model (3) to determine the electric resistance of the contact clusters for a given load. The contact-cluster configurations for each load results from a single simulation within model (1) and multiple simulations for different indentation zones on experimental surface, which are obtained with model (2). The detailed description of this multiscale resolution scheme will be soon available in [47].

The contact resistance obtained within this multiscale model is depicted in Fig. 9 and compared with experimental

data. To estimate the variability of the results, model (2) was used to simulate indentation at 100 different locations for contact radii ranging from 2 to 30 μm with step of 2 μm . The rigid stamp was squeezed on the substrate in 200 load steps; however, for the analysis only those simulation points were retained, for which the resulting force lies within a 5% interval of the force predicted by model (1). Two results of model (2) were retained for this analysis with $\sigma_y=53$ MPa and $\sigma_y=550$ MPa.

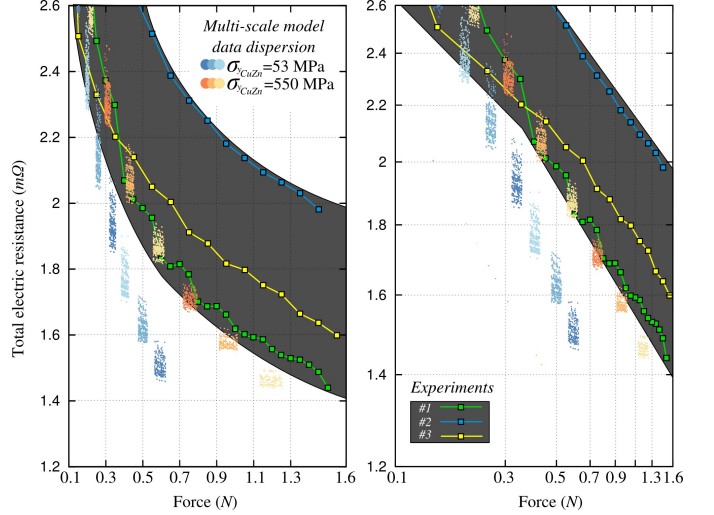


Fig. 9. Comparison between the actual multiscale model (clusters of points: blue for $\sigma_y=53$ MPa and red for $\sigma_y=550$ MPa) and experimental results (the shaded area represents the range of experimental results for the first loading, three distinct curves for the first loading are also shown). Different clusters of points correspond to different contact radii ($a=18, 20, 22, 24, 26$ and 28 μm).

Fig. 10 shows examples of contact spot configurations calculated with the model for the contact radius $a=10, 16$ and 22 μm . The anisotropy of the surface is easily observed – contact spots are localized along several bands. One can see that for higher values of the contact areas the a -spots grow beyond the delimited space and start to merge. At this stage the validity of models (2) and (3) becomes questionable and a finer analysis would be required. Integration of more realistic asperity deformations in model (2) could improve significantly the precision of predictions. This can be done by carrying out a series of finite element simulation of squeezing axisymmetric asperities with various geometrical parameters and subsequently fitting their response (displacement-force-contact radius) by simple polynomial curves, which can replace Hertz formula in model (2), as was done in [26]. Moreover, a further improvement of this feature, will make possible the simulation of cyclic loading on rough surfaces.

VII. CONCLUSION

In experiments, we identified a model-cycle (resistance with respect to load) for moderate loads which consists in a first distinct loading curve and subsequent unloading-loading cycles, for which the resistance follows separate but stabilized trajectories for unloading and loading paths (see Fig. 3). The stabilized loading-unloading cycle with a pronounced

hysteresis, comes from a kinematic hardening in the brass substrate. To capture the non-linear material behavior, our mechanical finite element analysis uses adequate material models, which include kinematic and isotropic hardening for isotropic J2-plasticity [48]. In agreement with experiments, it enables us to distinguish between the first loading and the subsequent cycles, however, the stabilized hysteresis, found in experiments, was not reproduced in simulations for various material parameters. The electrical contact resistance evaluated at macroscopic scale under assumption of perfectly conducting interface does not display a stabilized cycle for the range of tested material and geometrical parameters (see Fig. 5). Such a strong hysteresis should be associated with kinematic hardening of the brass at macroscopic scale and of CuBe and Au at the scale of asperities. Frictional dissipation and adhesion may also contribute to this hysteresis. For the subsequent studies, the frictional contribution has to be considered and all material models have to be more properly adjusted especially in terms of the kinematic hardening. However, in the framework of the currently used asperity based model, the cyclic elasto-plastic deformation at asperity scale cannot be properly taken into account, which is also the case for most elasto-plastic models.

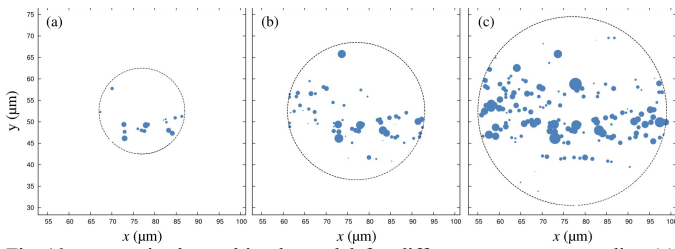


Fig. 10. a -spots in the multiscale model for different contact spot radius ($a=10 \mu\text{m}$, (b) $a=16 \mu\text{m}$, (c) $a=22 \mu\text{m}$).

The roughness of the studied surface (rolled brass coated with nickel and gold), while being frequently encountered in real world applications, is not typical for theoretical models, in which roughness is often assumed to be fractal, Gaussian and isotropic. The surface in this work obeys none of these assumptions and requires an accurate characterization and interpretation. For example, the contact spots, aligned in the rolling direction, form contact (conducting) bands separated by non-contact regions (see Fig. 10).

Comparison between the three-level computational model proposed in the paper and experiments shows that the model captures quantitatively the evolution of the electrical contact resistance during the first loading. However, it cannot predict the large variability of experimentally obtained results (this is probably because of too different finishes of the ball used in experiments). On the contrary, the model predicts the narrowing of the resistance values dispersion with increasing load, while in the experiments the variability remains large for high loads (compare dots with shaded area in Fig. 9). There are several reasons for this discrepancy:

1. apart from the contact roughness, the contact resistance is also associated with possible presence of oxide

films or other contamination on contacting surfaces: the electrical contact area is not equivalent to the mechanical contact area and can be significantly smaller in presence of poorly conducting spots [9];

2. the roughness and the surface state of the CuBe ball was neglected (probably it is the most critical approximation);
3. the passage from the finite element macroscopic result to the asperity based model requires a lot of assumptions, which in realistic case are only partly satisfied (see Section IV);
4. the asperity based model cannot take into account the merge of contact zones associated with different asperities [49] and the curvature variation of asperities;
5. Hertz contact theory even being extended to elasto-plastic material behavior cannot take into account the layered composition of the substrate and the finite strain hardening as well as it cannot capture a cyclic loading with kinematic hardenings.

To avoid the oversimplification of the elasto-plastic Hertz contact used for asperities, one may use a properly tuned heuristic model based on a series of finite element simulations of a single asperity on a layered substrate [26]. To overcome the ensemble of the aforementioned difficulties of the multiscale model a full scale finite element [26] or boundary element model for elasto-plastic material [50] (or their combination) with an accurate representation of the surface roughness should be used. This mechanical model should be complemented with a subsequent full scale finite element simulation of the current flux through the contact interface similar to what was done in [31]. However, to solve properly both the mechanical and electric problems at the roughness scale, a significantly finer meshes would be needed, see discussions in [22,51]. This task appears realistic in the present state of hardware and finite element software.

Note that such a weak electro-mechanical coupling is possible only for low electric currents as the Joule heating in the interface is negligibly small and thus does not affect material properties of contacting elements. However, when considering high electric currents a strongly coupled thermo-electro-mechanical model with roughness should be introduced similar to [31].

Finally, regardless all inherent drawbacks, the three-level multiscale and multiphysics model for electrical contacts yields reasonable results in good agreement with experiments. The model uses the real roughness topography and has no adjustable parameters, only material mechanical and electrical properties.

ACKNOWLEDGMENT

This work has benefited from the financial support of the LabeX LaSIPS (ANR-10-LABX-0040-LaSIPS) managed by the French National Research Agency under the "Investissements d'avenir" program (n°ANR-11-IDEX-0003-02).

REFERENCES

- [1] R. Holm, "Electrical Contacts, Theory and Applications," Springer-Verlag, Berlin, 1967.
- [2] R. Timsit, "The potential distribution in a constricted cylinder," *Journal of Physics D: Applied Physics*, vol. 10, no. 15, pp. 2011-2017, 1977.
- [3] J.A. Greenwood, "Constriction resistance and the real area of contact," *British Journal of Applied Physics*, vol. 17(12) pp. 1621-1632, 1966.
- [4] R.D Malucci, "Multispot model of contacts based on surface features," In *Electrical Contacts. Proceedings of 36th IEEE Holm Conference on*, pp. 625-634, 1990.
- [5] I. Minowa, and M. Nakamura, "Simulation for the current density distribution in a contact spot," *Electronics and Communications in Japan (Part II: Electronics)*, vol. 77(2) pp. 88-95, 1994.
- [6] L. Boyer, S. Noël, and F. Houzé, "Constriction resistance of a multispot contact: an improved analytical expression," In *Electrical Contacts. Proceedings of the 36th IEEE Holm Conference on*, and the 15th International Conference on Electrical Contacts, pp. 646-650. IEEE, 1990.
- [7] L. Boyer, "Contact Resistance Calculations: Generalizations of Greenwood's Formula Including Interface Films," *IEEE Transactions on Components and Packaging Technologies*, vol. 24(1), pp. 50-58, 2001.
- [8] Y.H. Jang, J.R. Barber, "Effect of contact statistics on electrical contact resistance," *Journal of Applied Physics*, vol. 94(11), pp. 7215-7221, 2003.
- [9] R. S. Timsit, "Electrical contact resistance: Fundamental principles," in *Electrical Contacts: Principles and Applications*, P. G. Slade, Ed. CRC Press, pp. 3-111, 2013.
- [10] J.A. Greenwood, J.B.P. Williamson, "Contact of nominally flat surfaces," *Proceedings of the Royal Society of London. Series A: Mathematical, Physical and Engineering Sciences*, vol. 295, pp. 300-319, 1966.
- [11] A.W. Bush, R.D. Gibson, T.R. Thomas, "The elastic contact of a rough surface," *Wear*, vol. 35(1), pp. 87-111, 1975.
- [12] T.R. Thomas, "Rough Surfaces," 2nd edition, Imperial College Press, 1999.
- [13] L. Afferrante, G. Carbone, G. Demelio, "Interacting and coalescing Hertzian asperities: a new multiasperity contact model," *Wear*, vol. 278-279, pp. 28-33, 2012.
- [14] M.S. Longuet-Higgins, "Statistical properties of an isotropic random surface," *Philosophical Transactions of the Royal Society A: Mathematical, Physical & Engineering Sciences*, vol. 250, pp. 157-174, 1957.
- [15] P.R. Nayak, "Random process model of rough surfaces," *Journal of Lubrication Technology (ASME)*, vol. 93, pp. 398-407, 1971.
- [16] W.E. Wilson, S.V. Angadi, and R.L. Jackson, "Surface separation and contact resistance considering sinusoidal elastic-plastic multi-scale rough surface contact," *Wear*, vol. 268(1), pp. 190-201, 2010.
- [17] B.N.J Persson, "Theory of rubber friction and contact mechanics. *Journal of Chemical Physics*, vol. 115, 3840-3861, 2001.
- [18] C. Yang, B.N.J. Persson, "Contact mechanics: contact area and interfacial separation from small contact to full contact," *Journal of Physics: Condensed Matter*, vol. 20(21), pp. 215214, 2008.
- [19] M. Paggi, M. Ciavarella, "The coefficient of proportionality k between real contact area and load, with new asperity models," *Wear*, vol. 268, pp. 1020-1029, 2010.
- [20] G. Carbone, F. Bottiglione, "Asperity contact theories: do they predict linearity between contact area and load?" *Journal of the Mechanics and Physics of Solids*, vol. 56, pp. 2555-2572, 2008.
- [21] C. Campañá, M.H. Müser, "Practical Green's function approach to the simulation of elastic semi-infinite solids, *Physical Review B*, vol. 74, pp. 075420, 2006.
- [22] L. Pastewka, N. Prodanov, B. Lorenz, M.H. Müser, M.O. Robbins, B.N.J. Persson, "Finite-size scaling in the interfacial stiffness of rough elastic contacts, *Physical Review E*, vol. 87, pp. 062809, 2013.
- [23] C. Putignano, L. Afferrante, G. Carbone, G. Demelio, "A new efficient numerical method for contact mechanics of rough surfaces," *International Journal of Solids and Structures*, vol. 49(2), pp. 338-343, 2012.
- [24] C. Putignano, G. Carbone, "A review of boundary elements methodologies for elastic and viscoelastic rough contact mechanics," *Physical Mesomechanics*, vol. 17(4), pp. 321-333, 2014.
- [25] L. Pei, S. Hyun, J.F. Molinari, M. Robbins, "Finite element modeling of elasto-plastic contact between rough surfaces," *Journal of the Mechanics and Physics of Solids*, vol. 53, pp. 2385-2409, 2005.
- [26] V.A. Yastrebov, J. Durand, H. Proudhon, and G. Cailletaud, "Rough surface contact analysis by means of the finite element method and of a new reduced model," *Comptes Rendus Mécanique*, vol. 339(7), pp. 473-490, 2011.
- [27] V.A. Yastrebov, G. Ancaix, J.F. Molinari, "From infinitesimal to full contact between rough surfaces: evolution of the contact area," *International Journal of Solids and Structures*, vol. 52, pp. 83-102, 2015.
- [28] R.D. Malucci, "Multi-spot model showing the effects of nano-spot sizes," In *Electrical Contacts. Proceedings of the 51st IEEE Holm Conference on*, pp. 291-297. IEEE, 2005.
- [29] A. Majumdar, C. Tien, "Fractal network model for contact conductance," *Journal of Heat Transfer*, vol. 113(3), pp. 516-525, 1991.
- [30] B. Arrazat, P.Y. Duvivier, V. Mandrillon, and K. Inal, "Discrete analysis of gold surface asperities deformation under spherical nano-indentation towards electrical contact resistance calculation," In *Electrical Contacts. Proceedings of the 57th Holm Conference on*, pp. 1-8. IEEE, 2011.
- [31] P. Shanthraj, O. Rezvanian, and M.A. Zikry, "Electrothermomechanical finite-element modeling of metal microcontacts in MEMS," *Journal of Microelectromechanical Systems*, vol. 20(2), pp. 371-382, 2011.
- [32] M. Myers, M. Leidner, H. Schmidt, H. Schlaak, "Extension and Experimental Verification of a New 'First Contact' Method to Model Performance of Multilayer Contact Interfaces," In *Electrical Contacts. Proceedings of the 54th IEEE Holm Conference on*, 1-8. IEEE, 2008.
- [33] R.L. Jackson, R.D. Malucci, S. Angadi, J.R. Polchow, "A Simplified Model of Multiscale Electrical Contact Resistance and Comparison to Existing Closed Form Models," In *Electrical Contacts. Proceedings of the 54th IEEE Holm Conference on*, 2009.
- [34] S. Lee, H. Cho, Y.H. Jang, "Multiscale electrical contact resistance in clustered contact distribution," *Journal of Physics D: Applied Physics*, vol. 42, pp. 165302-165309, 2009.
- [35] J.R. Barber, "Bounds on the electrical resistance between contacting elastic rough bodies," *Proceedings of the Royal Society of London. Series A: Mathematical, Physical and Engineering Sciences*, vol. 459(2029), pp. 53-66, 2003.
- [36] M.M. Yovanovich, "Four decades of research on thermal contact, gap, and joint resistance in microelectronics," *IEEE Transactions on Components and Packaging Technologies*, vol. 28(2), pp. 182-206, 2005.
- [37] C.V. Madhusudana, "Thermal contact conductance," Springer, 2nd edition, 2014.
- [38] J. Besson, and R. Foerch, "Large scale object-oriented finite element code design," *Computer Methods in Applied Mechanics and Engineering*, vol. 142(1), pp. 165-187 , 1997.
- [39] <http://www.zset-software.com/>
- [40] S. Guessab, L. Boyer, F. Houzé, S. Noël, and O. Schneegans, "Influence of temperature and pressure on the static contact resistance of vacuum heat-treated polyacrylonitrile films," *Synthetic metals*, vol. 118(1), pp. 121-132, 2001.
- [41] J.V. Carstensen, "Structural Evolution and Mechanisms of Fatigue in Polycrystalline Brass," PhD thesis, Riso National Laboratory, Roskilde, Denmark, 1998.
- [42] J.H. Kim, A. Nizami, Y. Hwangbo, B. Jang, H.J. Lee, C.S. Woo et al. "Tensile testing of ultra-thin films on water surface," *Nature communications* vol. 4, 2013.
- [43] R. Schwaiger, B. Moser, M. Dao, N. Chollacoop, and S. Suresh, "Some critical experiments on the strain-rate sensitivity of nanocrystalline nickel," *Acta materialia*, vol 51(17) pp. 5159-5172, 2003.
- [44] P.R. Nayak, "Random process model of rough surfaces in plastic contact," *Wear*, vol. 26, pp. 305-333, 1973.

- [45] J.A. Greenwood, "A simplified elliptic model of rough surface contact," *Wear*, vol.261, pp. 191-200, 2006.
- [46] Z. Song, K. Komvopoulos, "Elastic-plastic spherical indentation: deformation regimes, evolution of plasticity, and hardening effect," *Mechanics of Materials*, vol. 61, pp. 91-100, 2013.
- [47] F.S. Mballa Mballa, V.A. Yastrebov, G. Cailletaud, S. Noël, F. Houzé, and Ph. Testé, "Electric Contact: Experiments and Multiscale Electro-Mechanical Simulations," unpublished.
- [48] J. Besson, G. Cailletaud, J.L. Chaboche, and S. Forest, "Non-linear mechanics of materials," Springer, 2009.
- [49] J.A. Greenwood, "A note on Nayak's third paper," *Wear*, vol. 262(1), pp. 225-227, 2007
- [50] C. Jacq, D. Nelias, G. Lormand, and D. Girodin, "Development of a three-dimensional semi-analytical elastic-plastic contact code," *Journal of Tribology*, vol. 124(4), pp. 653-667, 2002.
- [51] V.A. Yastrebov, G. Anciaux, J.F. Molinari, "Contact between representative rough surfaces," *Physical Review E*, vol. 86(3), pp.035601, 2012.